Mon. Not. R. Astron. Soc. **298,** 1145–1158 (1998)

Measuring Ω_0 using cluster evolution

Vincent R. Eke,[1] Shaun Cole,[2] Carlos S. Frenk[2] and J. Patrick Henry[3]

[1] *Institute of Astronomy, University of Cambridge, Madingley Road, Cambridge CB3 0HA*
[2] *Department of Physics, University of Durham, South Road, Durham DH1 3LE*
[3] *Institute for Astronomy, 2680 Woodlawn Drive, Honolulu, HI 96822, USA*

Accepted 1998 April 8. Received 1998 March 2

ABSTRACT

The evolution of the abundance of galaxy clusters depends sensitively on the value of the cosmological density parameter, Ω_0. Recent *ASCA* data are used to quantify this evolution as measured by the cluster X-ray temperature function. A χ^2 minimization fit to the cumulative temperature function, as well as a maximum-likelihood estimate (which requires additional assumptions about cluster luminosities), leads to the estimate $\Omega_0 \approx 0.45 \pm 0.25$ (1σ statistical error). Various systematic uncertainties are considered, none of which significantly enhances the probability that $\Omega_0 = 1$. These conclusions hold for models with or without a cosmological constant, i.e., with $\Lambda_0 = 0$ or $\Lambda_0 = 1 - \Omega_0$. The statistical uncertainties are at least as large as any of the individual systematic errors that have been considered here, suggesting that additional temperature measurements of distant clusters will allow an improvement in this estimate. An alternative method that uses the highest redshift clusters to place an upper limit on Ω_0 is also presented and tentatively applied, with the result that $\Omega_0 = 1$ can be ruled out at the 98 per cent confidence level. Whilst this method does not require a well-defined statistical sample of distant clusters, there are still modelling uncertainties that preclude a firmer conclusion at this time.

Key words: galaxies: clusters: general – cosmology: theory.

1 INTRODUCTION

Galaxy clusters are the largest virialized objects in the Universe and, as such, provide useful cosmological probes. For example, the evolution in the abundance of clusters is strongly dependent on, and is therefore a sensitive probe of, the cosmological density parameter, Ω_0, (e.g. Evrard 1989; Frenk et al. 1990; Lilje 1992; Oukbir & Blanchard 1992).

The amount of observational data on high-redshift clusters has increased significantly in recent years. *EMSS* (Henry et al. 1992; Gioia & Luppino 1994), *ASCA* (e.g. Donahue 1996; Henry 1997; Mushotzky & Scharf 1997) and *ROSAT* (Burke et al. 1997; Ebeling et al. 1997; Rosati et al. 1998) measurements of the X-ray-emitting intracluster plasma now complement the low-redshift studies carried out by Edge et al. (1990) and David et al. (1993). In addition, the *CNOC* survey provides galaxy velocity dispersions for a well-defined sample of high-redshift clusters (Carlberg et al. 1996), and further information on mass distributions is coming from weak gravitational lensing measurements (e.g. Luppino & Kaiser 1997; Smail et al. 1997).

The modelling of the cluster population has relied heavily upon the expression provided by Press & Schechter (1974) for the mass function of haloes. This has received support from dark matter simulations of structure formation (e.g. Efstathiou et al. 1988; White, Efstathiou & Frenk 1993; Lacey & Cole 1994). More recently, the treatment of a baryonic component in simulations has led to a closer link with observational measurements (Evrard 1990; Bryan et al. 1994; Cen & Ostriker 1994; Metzler & Evrard 1994; Navarro, Frenk & White 1995, hereafter NFW; Frenk et al. 1996). In addition, analytical work investigating the evolution of properties of the cluster population as a whole has been performed by Kaiser (1986, 1991), Evrard & Henry (1991) and Bower (1997).

There is now sufficient overlap between these strands of research to allow useful conclusions concerning cosmological parameters to be drawn from the available data (see, however, Colafrancesco, Mazzotta & Vittorio 1997). Several groups have already attempted this operation (Henry 1997; Carlberg et al. 1997b; Bahcall, Fan & Cen 1997; Sadat, Blanchard & Oukbir 1998; Blanchard & Bartlett 1998; Reichart et al. 1998), although the lack of consensus on the measured value for Ω_0 casts doubt on the reliability of at least some of these studies. The purpose of this paper is to investigate the systematic uncertainties in the estimation of Ω_0 using cluster evolution, and to understand why the various studies differ.

In Section 2 the cosmology-dependent model for calculating the evolution of the cluster population is described. The procedure for and results from fitting the models to the observed temperature functions are presented in Section 3. Section 4 contains a description of a maximum-likelihood method used to estimate cosmological parameters from the measured cluster redshifts and temperatures. The results from these two methods are compared

with other studies in Section 5. In Section 6 an investigation is presented of how order statistics may be used to constrain Ω_0 from observations of one or more extreme objects at high redshift. A discussion of the different techniques is presented in Section 7. The implications of these results for $\Omega_0 = 1$ scenarios are discussed in Section 8, and conclusions are summarized in Section 9.

2 MODEL

The model of the population of hot galaxy clusters employed here is the same as the one described by Eke, Cole & Frenk (1996). This is based upon the analytical expression for the comoving number density of dark matter haloes first derived by Press & Schechter (1974):

$$\frac{\mathrm{d}n}{\mathrm{d}M_{\rm vir}} = \left(\frac{2}{\pi}\right)^{\frac{1}{2}} \frac{\bar{\rho}}{M_{\rm vir}^2} \frac{\delta_{\rm c}(z)}{\sigma} \left|\frac{\mathrm{d}\ \ln \sigma}{\mathrm{d}\ \ln\ M_{\rm vir}}\right| \exp\left[-\frac{\delta_{\rm c}(z)^2}{2\sigma^2}\right]. \quad (2.1)$$

Here $M_{\rm vir}$ denotes the halo virial mass, defined such that a halo has a mean density $\Delta_{\rm c}$ times the critical density at redshift z, where $\Delta_{\rm c}$ is evaluated using the spherical collapse model; $\bar{\rho}$ represents the present-day mean density of the Universe, and $\sigma(M_{\rm vir})$ the present-day, linear-theory rms density fluctuation in spheres containing a mean mass $M_{\rm vir}$. Throughout this paper, we use the fit to the cold dark matter power spectrum of Bardeen et al. (1986). The shape of the power spectrum and its amplitude at $8\,h^{-1}$ Mpc are described by σ_8 and Γ respectively (Efstathiou, Bond & White 1992). The spherical collapse threshold, δ_c, is employed for most of the analysis in the rest of this paper. Bryan & Norman (1998) report that their work, combined with the majority of published results, suggests that a slightly (< 10 per cent) higher value provides a better fit to mass functions from dark matter simulations. However, the recent simulations of Tozzi & Governato (1998) appear to support a lower value. This will be considered further in Section 8. Monaco (1998) has provided a review of the present understanding of the mass function.

An additional crucial ingredient in the model is the conversion from virial mass to emission-weighted X-ray temperature:

$$kT_{\rm gas} = \frac{7.75}{\beta_{\rm TM}} \left(\frac{6.8}{5X+3}\right) \left(\frac{M_{\rm vir}}{10^{15}\,h^{-1}\mathrm{M}_\odot}\right)^{\frac{2}{3}} \times (1+z) \left(\frac{\Omega_0}{\Omega(z)}\right)^{\frac{1}{3}} \left(\frac{\Delta_{\rm c}}{178}\right)^{\frac{1}{3}} \mathrm{keV}. \quad (2.2)$$

In this equation, $\beta_{\rm TM}$ is a conversion factor, the numerical value of which will be discussed shortly, and X is the hydrogen mass fraction, which is taken to be $X = 0.76$. If the specific galaxy kinetic energy equals the specific gas thermal energy within the virial radius, then a value of $\beta_{\rm TM} = 1$ would be appropriate for an isothermal gas. Alternatively, this value follows from applying hydrostatic equilibrium at the virial radius and assuming both that the sum of the logarithmic derivatives of the gas density and temperature profiles at this radius is -2, and that the gas temperature at this radius equals the overall emission-weighted value. Neither of these reasons is particularly persuasive. First, there is likely to be some residual kinetic energy in the gas as a result of incomplete thermalization (Evrard 1989). Secondly, numerical simulations show that the gas density is dropping off faster than r^{-2} at the virial radius, and that the temperature is also decreasing rather than remaining constant (e.g. NFW). The value of $\beta_{\rm TM}$ chosen here is based solely upon the results of hydrodynamical cluster simulations. These usually include shock heating but no radiative cooling or heating from any source. Such experiments

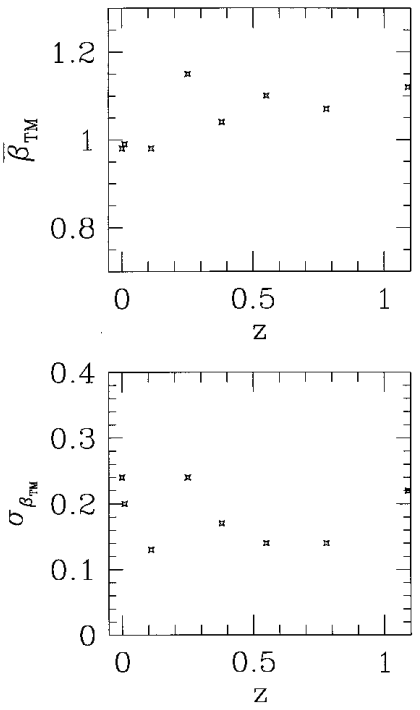

Figure 1. The top panel shows the evolution with redshift of the parameter β_{TM}, relating the emission-weighted X-ray temperature to the halo mass, as measured from an ensemble of 10 high-resolution hydrodynamical simulations of an $\Omega_0 = 0.3, \Lambda_0 = 0.7$ cosmology (Eke et al. 1998). The lower panel shows the standard deviation of the individual cluster β_{TM} values about this mean value as a function of redshift.

(NFW; Evrard, Metzler & Navarro 1996; Bryan & Norman 1998; Eke, Navarro & Frenk 1998; Frenk et al. 1998) suggest that $\beta_{\rm TM} = 1.0$ is a reasonable choice, and it is adopted as the default value in this paper, although the dependence of the results on this assumption will be investigated in Section 4. Values returned from different types of hydrodynamical simulations for a variety of cosmologies range between 1 and 1.3 (see Bryan & Norman 1998), with a slight preference for larger values of $\beta_{\rm TM}$ when Ω_0 is larger. No significant mass dependence of $\beta_{\rm TM}$ is found.

The redshift dependence of the mean value of $\beta_{\rm TM}$ for the 10 clusters simulated by Eke et al. (1998), and the scatter among the individual cluster values are shown in Fig. 1. Most importantly for estimating Ω_0 from cluster evolution out to $z \sim 0.4$, there is no significant evolution either in the mean $\beta_{\rm TM}$ or in the magnitude of the scatter about this value. As the temperature function has such a steep dependence on cluster temperature, uncertainties and possible biases in the mass–temperature conversion are very important (e.g. Pen 1998). A Gaussian scatter of 20 per cent in the temperature at a given mass has been included, consistent with Fig. 1, when calculating the model predictions. The neglect of physical processes associated with galaxy formation in hydrodynamical simulations of clusters is a concern, but the work of Metzler & Evrard (1994) suggests that even extreme feedback from stellar evolutionary effects cannot heat the intracluster medium of a rich cluster by more than about 15 per cent. Similarly, NFW found that $\beta_{\rm TM}$ was decreased by about 20 per cent if pre-heating was included in rich cluster simulations in order to match the slope of the observed luminosity–temperature relation. Hjorth, Oukbir & van Kampen (1998) find good agreement between deprojected weak lensing masses and X-ray masses for a sample of eight clusters. The study

by White (1991) comparing observed velocity dispersions with temperatures is also suggestive that non-gravitational processes have a relatively small effect on rich clusters. In Section 8 the possible extent to which the results presented here might depend upon physics missing from the numerical simulations will be considered further.

3 EVOLUTION OF THE CLUSTER TEMPERATURE FUNCTION

3.1 Estimating the cumulative temperature functions

The cluster X-ray emission-weighted temperature measurements that are used here come from two different sources. At low redshift, an updated version of the flux-limited [$f(2-10\,\mathrm{keV}) > 3\times10^{-14}$ W m^{-2}][1] sample of 25 clusters compiled by Henry & Arnaud (1991, hereafter HA91) is employed (see Henry, in preparation, for details). These authors report that this sample is 'at least 90 per cent complete'. In this section a completeness of 100 per cent will be assumed, but the effect of this uncertainty will be investigated further in Section 4. The average 1σ measurement uncertainty in these temperatures is 7 per cent. For the high-redshift data, the 10 *EMSS* $0.3 < z < 0.4$ cluster temperatures obtained by Henry (1997) are employed. These have an average 1σ uncertainty of 14 per cent. No systematic differences are found between these results and those of Mushotzky & Scharf (1997) for the five clusters in common.

In each case the cumulative cluster temperature function is estimated using

$$N(>kT) = \sum_{kT_i>kT} 1/V_{\mathrm{max},i}, \tag{3.1}$$

where $V_{\mathrm{max},i}$ is the maximum volume in which cluster i could be detected, given the survey selection criteria, and is calculated using the cluster fluxes and redshifts. A complication for the high-z sample is that the area of sky surveyed was a function of the sensitivity, i.e., only a small fraction of the total survey area was observed at the lowest flux levels. Using the data in table 3 of Henry et al. (1992), the following expression has been found to give the area of sky, A, in which a cluster providing a detect cell flux, f_{det}, would have been detectable by the *EMSS*:

$$\frac{A(f_{\mathrm{det}})}{A_{\mathrm{tot}}} = 1 - 3.05\,\mathrm{e}^{-0.41 f_{\mathrm{det}}} + 2.30\,\mathrm{e}^{-0.77 f_{\mathrm{det}}}. \tag{3.2}$$

Here f_{det} is in units of 10^{-16} W m^{-2}, and A_{tot} is the maximum area covered by the *EMSS* cluster survey, 735 deg^2. This fit is accurate to within 10 per cent at all detect cell fluxes above the Henry (1997) catalogue limit of 2.5×10^{-16} W m^{-2}. Using the cluster detect cell fluxes and redshifts provided in table 1 of Henry (1997), the cluster flux can be calculated as a function of redshift. $V_{\mathrm{max},i}$ is then evaluated by integrating the product of dV/dz and fractional survey area at a particular redshift from $z = 0.3$ to 0.4.

Before this estimate of $N(>kT)$ can be compared with the model, a correction for incompleteness in the measured high-redshift temperature function is required. This arises because of the non-zero scatter in the luminosity–temperature relation and the fact that the high-redshift sample has a non-zero lower redshift limit. As a consequence, at the low-redshift limit of the sample, the flux limit of 2.5×10^{-16} W m^{-2} corresponds to a non-zero luminosity limit such that for any given temperature, only clusters with luminosities higher than this limit will be included. The incompleteness will be greater for cooler clusters because, on average, they have lower luminosities. To calculate the amplitude of this effect, the data of HA91 for low-redshift clusters were used to provide both a mean luminosity as a function of cluster temperature and a scatter about this mean. What observational evidence there is suggests that the luminosity–temperature relation evolves very little out to redshifts of 0.4 (Tsuru et al. 1996; Henry 1997; Mushotzky & Scharf 1997). This gave

$$\log_{10}\bar{L}_{37}^{0.3-3.5} = 3.54\,\log_{10}(kT) - 2.53, \tag{3.3}$$

where $\bar{L}_{37}^{0.3-3.5}$ is the 0.3–3.5 keV luminosity measured in $10^{37}\,h^{-2}$ W and kT is in units of keV, and a Gaussian scatter in $\log_{10} L_{37}^{0.3-3.5}$ of

$$\sigma = 0.69 - 0.47\,\log_{10}(kT). \tag{3.4}$$

At any given temperature, the fraction of clusters that are actually selected is then just given by

$$F(T, L_{\mathrm{lim}}) = 0.5\ \mathrm{erfc}[x_{\mathrm{lim}}(T)], \tag{3.5}$$

where erfc represents the complementary error function, $x_{\mathrm{lim}} = (\log_{10} L_{\mathrm{lim}} - \log_{10}\bar{L})/(\sqrt{2}\sigma)$ and L_{lim} is the (cosmology-dependent) luminosity of a cluster at $z = 0.3$ having a flux equal to f_{lim}. To allow for the fact that the catalogue flux limit refers to the *EMSS* detect cell whilst the clusters are typically more extended, a factor of 2.1 has been included to account for the conversion between these two fluxes (see fig. 1 of Henry et al. 1992). The product of $F(T, L_{\mathrm{lim}})$ and the differential number density at the same temperature can then be integrated with respect to temperature to give the correction to the cumulative temperature function. Even for temperatures as low as 4 keV the incompleteness is no more than 20 per cent. This can be seen in Fig. 2, where the low-redshift cumulative cluster temperature function is shown as a stepped line along with that from the high-z sample, calculated assuming that $\Omega_0 = 1$ and ignoring the incompleteness correction. The points represent the data used for the quantitative comparison with the models, and they include the correction factor which only has any significant effect on the lowest temperature measurement. The 1σ uncertainties on the number densities come from a bootstrap resampling procedure using 10^4

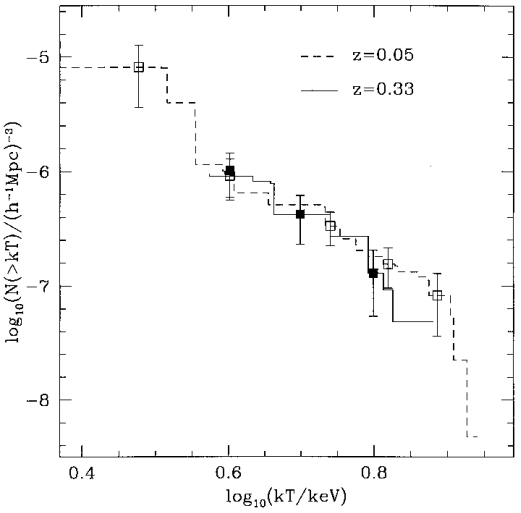

Figure 2. The stepped curves show the low- (dashed) and high- (solid) redshift cumulative cluster temperature functions, calculated assuming that $\Omega_0 = 1$. The points are the values that were used in the model fitting, and include the incompleteness correction for the high-redshift case. Open and filled symbols correspond to the low- and high-redshift data respectively. Error bars were computed using bootstrap resampling.

[1] For the benefit of older readers, 1 W $\equiv 10^7$ erg s^{-1}.

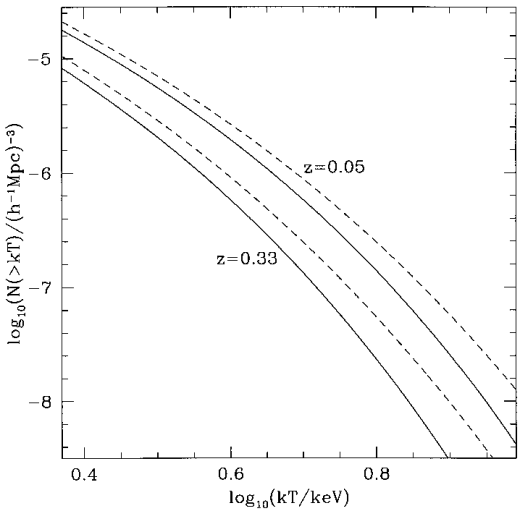

Figure 3. The predicted evolution of the cluster temperature function between $z = 0.05$ and 0.33 is shown for an $\Omega_0 = 1$ model with $\sigma_8 = 0.52$ and $\Gamma = 0.25$, both before (solid) and after (dashed) a Gaussian smoothing with width $0.2T$ has been applied.

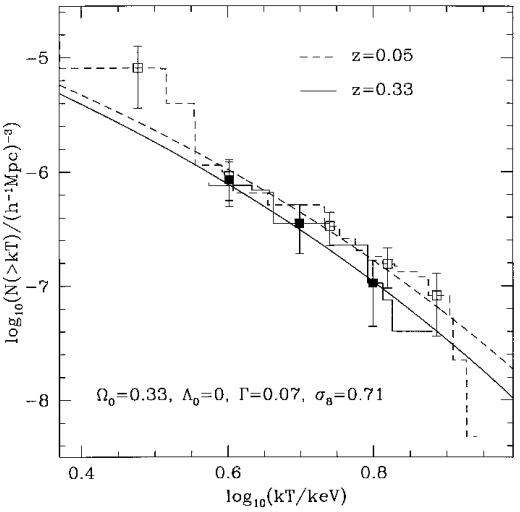

Figure 4. The best-fitting model and the corresponding data are shown for the $\Lambda_0 = 0$ case. Low- (high-) redshift data are represented with a dashed (solid) line and open (filled) squares as in Fig. 2.

catalogues. Poissonian distributions are used for the total numbers of clusters in the bootstrap catalogues (Markevitch 1998), rather than simply choosing (with replacement) 25 or 10 clusters for all low- and high-redshift catalogues respectively.

3.2 Comparison with model predictions

Given that the cumulative cluster number density varies rapidly with temperature, uncertainties in either the mass-to-temperature conversion or in the observed temperatures of individual clusters will impact more on the results than any minor incompleteness. These effects can both be modelled by smoothing the model temperature function before it is compared with observational data. The width of the smoothing function, which has been taken to be a Gaussian, has been estimated by adding the fractional uncertainties from the two sources in quadrature. From the results in Fig. 1, the scatter in individual cluster $\beta_{\rm TM}$ values is slightly less than 20 per cent, and it appears to be independent of redshift for $z < 0.4$. While these simulations were of an $\Omega_0 = 0.3$, $\Lambda_0 = 0.7$ model, in the absence of information to the contrary, this scatter is assumed to apply to other cosmological models as well. For both observational redshift ranges, the temperature uncertainties are sufficiently small compared with the scatter in $\beta_{\rm TM}$ that neglecting them will not affect the final results significantly. Therefore a Gaussian distribution of width $0.2T$, corresponding to the assumed scatter in $\beta_{\rm TM}$, was used. From Fig. 3 it is apparent that this correction is not negligible compared with the amount of evolution that the $\Omega_0 = 1$ model predicts. However, if the width of the Gaussian is similar for both the high- and low-redshift samples, then the amount of evolution is largely unaffected because the cumulative temperature function is almost a power law. The estimate of σ_8 will be decreased slightly by this effect. Compared with the rapid evolution in the number of clusters at a particular temperature, Fig. 3 illustrates how little the temperature at a fixed number density evolves, and how important any evolution in the mass–temperature relation is over this range of redshifts.

The model described by equations (2.1) and (2.2) has three free parameters; Ω_0, Γ and σ_8. The best-fitting values of these parameters were found by minimizing the value of χ^2 calculated at five and three temperatures in the low- and high-redshift bins respectively. Bin temperatures were chosen to be far apart, in order to reduce the correlations between the different points. Nevertheless, the full covariance matrix was employed when calculating the χ^2 values. The number of bins used was the minimum for which the results of the model fitting were found to be robust to the exact positioning of the bins. If any fewer bins are taken, then the results depend upon their chosen temperatures. This is particularly so for the low-redshift data, where the observed function is less smooth than in the high-redshift case. The statistical uncertainties in the best-fitting parameters were quantified using both the change in χ^2 and the distribution of best-fitting values from the 10^4 bootstrap catalogues that were created from the observational data.

3.3 Results

The χ^2 minimization gave the following best-fitting parameter values: $\Omega_0 = 0.33$, $\Gamma = 0.07$ and $\sigma_8 = 0.71$ for $\Lambda_0 = 0$, and $\Omega_0 = 0.27$, $\Gamma = 0.07$ and $\sigma_8 = 0.81$ for $\Lambda_0 = 1 - \Omega_0$. In the latter case, two different effects act in opposite directions on the most likely value of Ω_0 compared with the $\Lambda_0 = 0$ case. If Λ_0 is non-zero, then the expected amount of evolution at a particular Ω_0 increases because of the more rapidly changing fluctuation growth factor. However, the volume surveyed between redshifts 0.3 and 0.4 also increases if a $\Lambda_0 = 1 - \Omega_0$ term is included, and this has the effect of decreasing the observed cluster number density at high-redshift relative to the low-redshift measurement. Given that the most likely Ω_0 decreases, albeit only slightly, when Λ_0 is assumed to be non-zero, the former effect is the more important. The best-fitting curves for $\Lambda_0 = 0$, together with the observational data points, are shown in Fig. 4.

In order to assess the statistical uncertainties in the estimated parameters, one can consider both the contours of $\Delta\chi^2$ and the distributions of the best-fitting values of the bootstrap catalogues. It is interesting to look at both of these, because the χ^2 method formally assumes that the uncertainty in the estimated temperature function is Gaussian distributed, which is not fully justified, given the small number of clusters in the two samples. Fig. 5 shows the

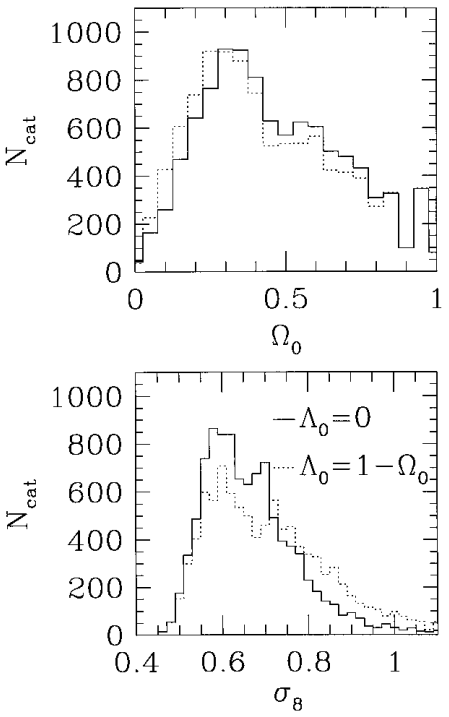

Figure 5. Histograms showing the distributions of the 10^4 bootstrap catalogue best-fitting Ω_0 and σ_8 values. Open and flat models are represented by solid and dotted lines respectively.

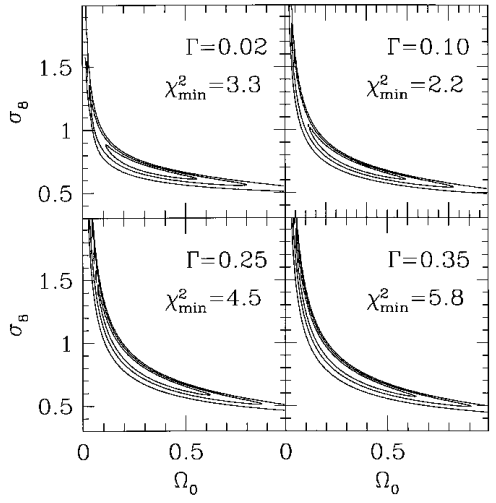

Figure 6. Contours of constant $\Delta\chi^2$ for slices in parameter space at fixed Γ, as given in the individual panels. The $\Delta\chi^2$ values shown are 2.30, 6.17 and 11.8 and, for two interesting parameters, these correspond to enclosed probabilities of 1, 2 and 3σ. All panels are for the $\Lambda_0 = 0$ models. In each case, the minimum χ^2 from all of the models with the chosen Γ is also given.

distribution of best-fitting bootstrap catalogue parameters. The open and flat models are represented by solid and dotted lines respectively. Figs 6 and 7 show slices through the three-dimensional parameter space at different values of Γ and Ω_0 respectively. The contour levels represent 1, 2 and 3σ contours for two degrees of freedom, i.e., not marginalized with respect to the parameter that is fixed. All panels are for open models with $\Lambda_0 = 0$. Very little changes with the inclusion of a non-zero Λ_0. The minimum values of χ^2 are given for each of the slices. Estimates of the uncertainties

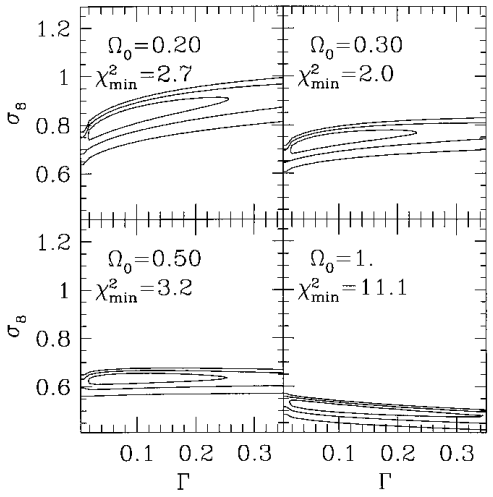

Figure 7. Contours of constant $\Delta\chi^2$ for slices in parameter space at fixed Ω_0, as given in the individual panels. The $\Delta\chi^2$ values shown are 2.30, 6.17 and 11.8 and, for two interesting parameters, these correspond to enclosed probabilities of 1, 2 and 3σ. All panels are for the $\Lambda_0 = 0$ models. In each case, the minimum χ^2 from all of the models with the chosen Ω_0 is also given.

have been obtained by looking at the cumulative distributions of the bootstrap catalogue best-fitting parameters. The following ranges contain 68 per cent of these values:

$$\Omega_0 = [0.23, 0.72], \quad \Gamma = [0.01, 0.14], \quad \sigma_8 = [0.56, 0.78] \qquad (3.6)$$

if $\Lambda_0 = 0$, and

$$\Omega_0 = [0.20, 0.72], \quad \Gamma = [0.01, 0.14], \quad \sigma_8 = [0.57, 0.88] \qquad (3.7)$$

if $\Lambda_0 = 1 - \Omega_0$. When the individual bootstrap catalogue best-fitting parameters were over-plotted on the $\Delta\chi^2$ contours shown in Figs 6 and 7, they were found to trace very similar patterns. Only a few lay outside the '3σ' contours, having Ω_0 values slightly larger than would be expected given these two figures. However, as is evident from Fig. 5, there are nevertheless very few catalogues favouring $\Omega_0 > 0.9$. This provides some reassurance that the $\Delta\chi^2$ contours are not providing a misleading impression of the statistical uncertainties in the various parameters, despite the low number of clusters per bin.

4 MAXIMUM-LIKELIHOOD PARAMETER ESTIMATION

One drawback of the method presented in the previous section is that the precise cluster redshifts are not employed, and so the modelling ignores any evolution within the redshift ranges spanned by the two data sets. In this section a maximum-likelihood technique is applied to determine the most likely model for producing the measured values of cluster temperatures and redshifts. This has the advantages over the previous method that no particular binning in temperature is required, and the individual cluster redshifts are used. The disadvantage is that the measured cluster fluxes are not included in the scheme, and additional assumptions about the cluster luminosities need to be made.

If $a(z, T)\mathrm{d}z\mathrm{d}T$ is the model probability of observing a cluster with temperature T at redshift z, then the likelihood of the observed distribution of cluster temperatures and redshifts can be written as

$$\mathcal{L} = \prod_{i=1}^{N} a_i \mathrm{d}z\mathrm{d}T \mathrm{e}^{-a_i \mathrm{d}z\mathrm{d}T} \prod_{j=N+1}^{N_{\mathrm{Tot}}} \mathrm{e}^{-a_j \mathrm{d}z\mathrm{d}T}. \qquad (4.1)$$

Here j is an index running over all those of the $N_{\rm Tot}$ total bins in redshift and temperature that are empty, and i runs over just the N bins occupied by the observed clusters. This equation follows from assuming that the cluster redshifts and temperatures are independent, and taking bins such that $a_i \ll 1 \forall i$. Neglecting the terms that do not depend upon the cosmological parameters, equation (4.1) can be written as

$$\ln \mathcal{L} = \sum_{i=1}^{N} \ln a_i - \int\int a \mathrm{d}z \mathrm{d}T. \tag{4.2}$$

The function $a(z, T)$ can be defined as

$$a(z,T) = n(z,T,p) \frac{\mathrm{dV}(z,p)}{\mathrm{d}z} \zeta(z,T,p), \tag{4.3}$$

where p represents the three model parameters being investigated, n is the comoving cluster number density given by the Press–Schechter-based model including a correction for the 20 per cent uncertainty in the mass–temperature conversion, V is the comoving volume, and ζ is the product of the fraction of sky surveyed and the estimated completeness of the survey. For the high-redshift catalogue, the fraction of sky surveyed has been calculated by integrating equation (3.2) over all possible fluxes at a given (z, T, p), thereby accounting for the scatter in the luminosity–temperature relation and the variation of sky covered as a function of flux in the *EMSS*. A single-temperature bremsstrahlung model has been used to calculate the 'K'-corrections to the cluster fluxes. The default temperature to luminosity conversions that have been employed are given by equation (3.3) for the 0.3–3.5 keV band and, again using the HA91 clusters,

$$\log_{10} \bar{L}_{37}^{2-10} = 3.93 \log(kT/\mathrm{keV}) - 2.92 \tag{4.4}$$

for the 2–10 keV band. The scatter in $\log_{10}$ (luminosity) about these relations is described by equation (3.4) and by

$$\sigma = 0.70 - 0.52 \log_{10}(kT/\mathrm{keV}) \tag{4.5}$$

respectively. To estimate how the choice of L–T conversion affects the results, the David et al. (1993) sample has also been considered, giving

$$\log_{10} \bar{L}_{37}^{0.3-3.5} = 2.76 \log(kT/\mathrm{keV}) - 2.02 \tag{4.6}$$

and

$$\log_{10} \bar{L}_{37}^{2-10} = 3.45 \log(kT/\mathrm{keV}) - 2.57. \tag{4.7}$$

As in the previous section, there is assumed to be no evolution in the luminosity–temperature relation.

The dependence of the best-fitting parameters on the following factors has been investigated: the assumed completeness of the low-redshift sample, the assumed conversion between cluster flux and *EMSS* detect cell flux, the luminosity–temperature conversions, and the amplitudes of the scatter about these mean relations. The default choice is to assume that both high- and low-redshift samples are 100 per cent complete. Note that a lower completeness for the high-redshift sample would give rise to lower estimates for Ω_0. Unless stated otherwise, a cluster at redshift z is taken to have $2.4 - z$ times as much flux as would fall into the *EMSS* detect cell (see fig. 1 of Henry et al. 1992). The redshift and temperature limits for the binning are chosen so as just to encompass all of the data points. For the low-redshift sample this means $2.5 < kT/\mathrm{keV} < 10$ and $0 < z < 0.1$, and for the high-redshift bins $3.7 < kT/\mathrm{keV} < 10$ and $0.3 < z < 0.4$. The region of parameter space that has been searched for the most likely parameters is $0.01 \leq \Omega_0 \leq 1$ (with $\Lambda_0 = 0$ or $1 - \Omega_0$), $0.01 \leq \Gamma \leq 0.25$ and $0.5 \leq \sigma_8 \leq 1.2$.

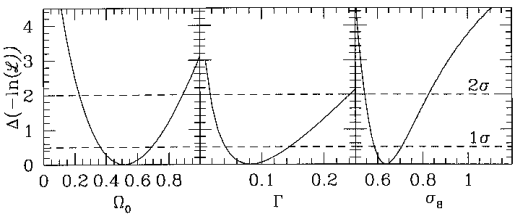

Figure 8. Δ (–ln likelihood)s for Ω_0 (left panel), Γ (middle) and σ_8 (right), marginalized over the other two parameters in each case. Dashed lines at 1 and 2σ significance are shown, and the top of each panel corresponds to 3σ for one interesting parameter. The default assumptions giving rise to these results are described in the text.

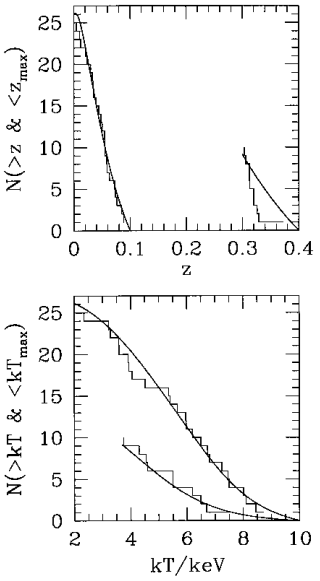

Figure 9. Marginalized data (stepped curves) and best-fitting model (smooth curves) for the redshift and temperature distributions of the clusters in the best-fitting model: $\Omega_0 = 0.52$ ($\Lambda_0 = 0$), $\Gamma = 0.08$ and $\sigma_8 = 0.63$.

4.1 Results

With the default assumptions described in the preceding section, the most likely parameter values are $\Omega_0 = 0.52$, $\Gamma = 0.08$ and $\sigma_8 = 0.63$ for the $\Lambda_0 = 0$ model. The statistical uncertainties on these parameters can be determined by considering the marginalized likelihoods. These one-dimensional likelihoods are shown for all three of the fitted parameters in Fig. 8. In each case the maximum likelihood is found at each value of the chosen parameter, independently of the other two parameters. Confidence levels are therefore taken for a single interesting parameter, leading to 1σ uncertainties of $\Omega_0 = 0.52^{+0.17}_{-0.16}$, $\Gamma = 0.08^{+0.07}_{-0.04}$ and $\sigma_8 = 0.63^{+0.08}_{-0.05}$. The model predictions for the marginalized number of clusters as a function of either redshift or temperature are shown in Fig. 9 for the most likely case. It is evident that the high-redshift sample cluster distribution is not very well matched by the model. In fact a Kolmogorov–Smirnov test indicates that the probability that this data set was produced from the model distribution is of order 10^{-3}. A comparison of *CNOC* (Carlberg, Yee & Ellingson 1997a) with *EMSS* (Henry et al. 1992) redshifts suggests that the low probability cannot be accounted for by redshift measurement errors. If the maximum redshift limit of the Henry (1997) cluster sample is decreased from 0.4 to 0.33 and the likelihoods are recomputed, then

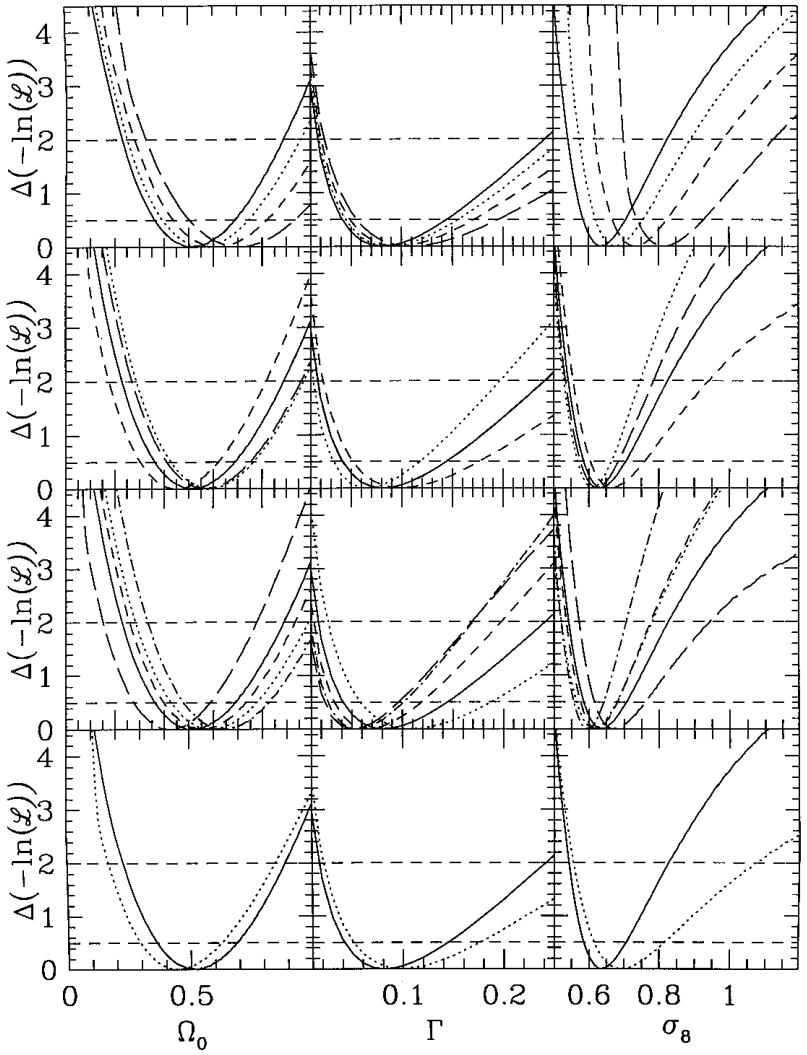

Figure 10. Δ (−ln likelihood)s for Ω_0 (left panels), Γ (middle) and σ_8 (right), marginalized over the other two parameters in each case. Dashed lines at 1 and 2σ significance are shown, and the top of each panel corresponds to 3σ for one interesting parameter. In all rows, the default curves shown in Fig. 8 are reproduced with solid lines. The top row shows curves for $\beta_{\rm TM} = 1.2$, 1.5 and 2 with dotted, short-dashed and long-dashed lines respectively. In the second row, the results of a cluster to *EMSS* detect cell flux ratio of $2 - z$ (dotted) and $2.8 - z$ (short dashed) are given along with results obtained by assuming that the low-redshift data are 10 per cent incomplete (long-dashed). Illustrated in the third row are curves resulting from decreasing the L–T scatter for the low-z sample by 30 per cent (dotted), increasing the scatter by 30 per cent for the high-z sample (short-dashed), using the different mean L–T relations described in equations (4.7) and (4.6) (long-dashed) or simply increasing the high-z luminosity at a given temperature by 50 per cent (dot-dashed). The final row shows the likelihoods found after assuming that $\Lambda_0 = 1 - \Omega_0$ (dotted).

the resulting Ω_0 becomes $\lesssim$0.13 (the best-fitting σ_8 is at least 1.2, which is the largest value considered on the grid of likelihoods). This suppression of the high-z survey volume with the corresponding removal of only one of the 10 clusters has the effect of reducing the apparent evolution and, likewise Ω_0. However, if the redshift distribution of the $z > 0.4$ *EMSS* clusters is also considered, then models with so little evolution will predict many more distant clusters than are observed. The redshift distribution of the $0.3 < z < 0.4$ clusters is therefore rather difficult to explain.

Fig. 10 shows the effect on the most likely parameters produced by altering the model assumptions. From top to bottom, the rows show the variation with (1) $\beta_{\rm TM}$, (2) survey incompleteness and uncertain $f_{\rm clus}/f_{\rm det}$, (3) L–T treatment, and (4) the inclusion of a non-zero Λ_0 term. Table 1 contains details of the most likely parameters in the different cases.

Increasing $\beta_{\rm TM}$ has the effect of boosting σ_8. This suppresses the

Table 1. Most likely parameters for the different input assumptions shown in Fig. 10.

Change from default choices	Ω_0	Γ	σ_8
none	0.52	0.08	0.63
$\beta_{\rm TM} = 1.2$	0.55	0.09	0.68
$\beta_{\rm TM} = 1.5$	0.61	0.10	0.73
$\beta_{\rm TM} = 2.0$	0.72	0.11	0.81
$f_{\rm clus}/f_{\rm det} = 2.0 - z$	0.59	0.07	0.61
$f_{\rm clus}/f_{\rm det} = 2.8 - z$	0.44	0.10	0.67
$z = 0$ sample 90 per cent complete	0.58	0.08	0.62
$z = 0$ L–T scatter $\times 0.7$	0.59	0.11	0.61
$z = 0.3 - 0.4$ L–T scatter $\times 1.3$	0.56	0.07	0.62
L–T given by eqns. (4.6) and (4.7)	0.43	0.05	0.67
$z = 0.3 - 0.4$ mean $L \mid T \times 1.5$	0.64	0.06	0.60
$\Lambda_0 = 1 - \Omega_0$	0.45	0.10	0.69

amount of evolution expected for any given Ω_0, thus leading to a higher estimate of the density parameter. It should be noted that a much more effective way of changing the most likely Ω_0 would be to have some *evolution* in the value of $\beta_{\rm TM}$, rather than merely changing the mean at all redshifts. Even $\beta_{\rm TM} = 2$, which seems rather extreme (see Section 8), only produces a $+0.2$ change in the density parameter.

The second row in Fig. 10 shows the relative insensitivity of the results to the assumed conversion between total cluster flux and *EMSS* detect cell flux, $\Delta\Omega_0 = \pm 0.08$ for extreme choices (see Henry et al. 1992, fig. 1). When the ratio $f_{\rm clus}/f_{\rm det}$ is taken to be larger, this corresponds to a need for more luminous clusters in the high-redshift sample and hence a lower value for Ω_0. A 10 per cent incompleteness in the low-redshift cluster sample enhances the evolution enough to give $\Omega_0 = 0.58$. However, if the high-redshift sample was less than 100 per cent complete, then the best-fitting value would decrease accordingly (see Section 8).

The scatter in the luminosity–temperature relations has been varied to see how much the most likely density parameter can be increased. In the third row of Fig. 10, it is apparent that very little impact is made with these alterations. More significant is the reduction in Ω_0 that comes from exchanging the L–T equations (4.6) and (4.7) for the default choices (3.3) and (4.4). This yields $\Omega_0 = 0.43$. The amplification of the high-redshift luminosity at a given temperature by 50 per cent, which is more than is observed (Tsuru et al. 1996; Henry 1997; Mushotzky & Scharf 1997), increases the number of clusters that should be seen further away. Consequently, to fit the observed abundance, it is necessary to increase the amount of evolution to compensate, giving a best-fitting $\Omega_0 = 0.64$.

As is evident from this figure, the best-fitting value of Ω_0 is difficult to change by more than $\sim$0.1 with any single one of these systematic changes. Additional reasons why these results might be misleading will be considered in Section 8, with particular emphasis on what can be said about the health of the critical density model in the light of cluster evolution.

The final row in Fig. 10 shows how the most likely parameters are affected by the inclusion of a $\Lambda_0 = 1 - \Omega_0$ term. In this case, the most likely parameters and 1σ marginalized uncertainties are $\Omega_0 = 0.45^{+0.18}_{-0.16}$, $\Gamma = 0.10^{+0.08}_{-0.05}$ and $\sigma_8 = 0.69^{+0.13}_{-0.08}$.

Of the systematic effects investigated above, only the choice of upper redshift limit for the Henry (1997) sample and the excessive change in $\beta_{\rm TM}$ manage to alter the most likely Ω_0 by much more than 0.15. However, the statistical uncertainties are sufficiently large that in none of the above cases is $\Omega_0 = 1$ ruled out with a significance of 3σ or greater.

5 COMPARISON WITH OTHER STUDIES

The analysis presented here produces results in good agreement with those of Henry (1997). This is not surprising, given that very nearly identical data have been employed, albeit within different modelling procedures. These results fit happily with the *ROSAT* log$N$–log$S$ analysis by Mathiesen & Evrard (1998) as long as the luminosity evolves like $L \propto (1+z)^{\sim 3}$. This is approximately what is implied by equations (2.2) and (3.3), although it should be noted that the results in Section 3 are almost completely insensitive to the assumed form of the L–T relation, unlike those in Section 4. Kitayama & Suto (1997) have also used the log$N$–log$S$ relation of X-ray clusters to arrive at the conclusion that $\Omega_0 = 0.45$ is favoured if $\Lambda_0 = 0$.

Of the other results in this field, there appears to be two more distinct camps, one on either side of the above settlement in the middle of Ω_0-space. On the lower side, though not by much, favouring $\Omega_0 \approx 0.40 \pm 0.12$ and 0.30 ± 0.10 are Carlberg et al. (1997b) and Bahcall et al. (1997) respectively. These results are consistent with those found here, although the small quoted uncertainties strongly imply that $\Omega_0 < 1$. The 'high-ground', with $\Omega_0 = 0.8-1$, is occupied by Sadat et al. (1998) and Blanchard & Bartlett (1998). At this point the reader might wonder why any of these conclusions concerning Ω_0 are worth taking seriously, given that they appear to be inconsistent and span the whole range of interesting values. That such disparate results are obtained is presumably a suggestion that unaccounted-for systematic errors are lurking beneath the surface in at least one of these analyses. As has been stressed in this paper, and was also discussed by Pen (1998), the cluster number density evolution is rapid if considered at a particular mass. However, at a fixed number density the mass varies relatively little over the range of redshifts probed by the presently available data. For instance, in an $\Omega_0 = 1$ model normalized to match the $z = 0$ cluster abundance, the evolution between $z = 0.05$ and 0.33 of the mass at a constant comoving cluster number density is $\sim$45 per cent. Any unaccounted-for relative systematic temperature errors (i.e., affecting the low- and high-redshift samples differently) must therefore be smaller than $\sim$30 per cent, or else the comparison between the models and observations will become completely unreliable. The quantification of any potential systematic uncertainties in mass estimation is thus crucial in determining the size of the error bar on the derived Ω_0.

For the studies producing lower Ω_0 determinations, velocity dispersions obtained using different procedures are used to estimate masses. Frenk et al. (1996) and van Haarlem, Frenk & White (1997) investigated the biases in mass estimation using velocity dispersions, and more recently Borgani et al. (1997) considered the model dependence of these biases. These studies suggest that only after very careful modelling of the velocity dispersion calculation procedure should this method be applied with any confidence. From the simple scaling laws $M \propto \sigma_{\rm v}^3$ and $M \propto T^{1.5}$, it is immediately apparent that fractional uncertainties in velocity dispersion would need to be half those in the X-ray temperature in order for the virial mass to be equally accurate. The importance of such conversions is shown by figs 1 and 2 of Carlberg et al. (1997b), where the higher redshift *CNOC* number density determination lies at a greater mass than the other *CNOC* point. This is slightly surprising, because the virial theorem suggests that the same velocity dispersion should be produced by equal masses out to a given physical radius, irrespective of redshift. Under the assumption that both *CNOC* redshift ranges have the same cluster mass limit, which was the choice made by Bahcall et al. (1997), the higher redshift *CNOC* point can be made to lie rather happily on the $\Omega_0 = 1$ model prediction shown in fig. 2 of Carlberg et al., as long as their high-redshift point is shifted to the mass limit of their low-redshift sample. While it is not clear that this is the correct mass to choose, and Bahcall et al. took an intermediate value, this demonstrates how sensitively the conclusions about Ω_0 depend on such details. In addition to these difficulties, the *CNOC* sample, which is almost a subsample of *EMSS* clusters and contains five from the high-redshift set studied by Henry (1997), has both a luminosity and a velocity dispersion cut. Consequently, when converting to an observed number density of clusters above a particular mass, a correction for scatter in the correlations between these properties is required. As Carlberg et al. (1997b) showed, this is uncertain by $\sim$50 per cent.

Bahcall et al. (1997) also consider the richnesses in the Palomar

Distant Cluster Survey. This is suspect because of the well-known difficulties associated with trying to calibrate the richness–mass correlation and, more importantly, any possible evolution in it (e.g. van Haarlem et al. 1997).

Moving on to the large-Ω_0 camp, Blanchard & Bartlett (1998) claim that their result 'in conjunction with the absence of any negative evolution in the luminosity–temperature relation, provides robust evidence in favour of a critical density universe'. The data used to draw this conclusion come from a variety of sources: *CNOC* velocity dispersions, *EMSS* luminosities and *ROSAT* luminosities. As these authors point out, there is considerable uncertainty in the number density of clusters above 6 keV at redshift zero. A consistent value of $\sim 30 \times 10^{-8} (h^{-1}\mathrm{Mpc})^{-3}$ is obtained from both the samples of Edge et al. (1990) and HA91. Integrating the *ROSAT* Brightest Cluster Sample (BCS) (Ebeling et al. 1997) best-fitting Schechter function for the *EMSS* passband (0.3–3.5 keV) from infinity to the luminosity corresponding to 6 keV ($1.25 \times 10^{37}\, h^{-2}$ W) suggests a number density of clusters of $\sim 40 \times 10^{-8} (h^{-1}\mathrm{Mpc})^{-3}$. The value calculated by Blanchard & Bartlett is twenty per cent greater than this. As a consequence of this larger redshift zero abundance, both the evolution of the cluster number density and the derived value of Ω_0 are increased. Despite this, figure 2 of Blanchard & Bartlett still does not provide particularly compelling evidence in favour of an $\Omega_0 = 1$ model.

Sadat et al. (1998) used the lack of evolution of the cluster luminosity–temperature relation to give a 'tentative' measurement of $\Omega_0 = 0.85 \pm 0.2$. This determination was based on an application of the method proposed by Oukbir & Blanchard (1997). They showed how, by using the redshift-zero cluster temperature function normalization and the redshift distribution of *EMSS* clusters, it was possible to relate Ω_0 to the evolution of the cluster luminosity–temperature relationship. However, as Sadat et al. note, Oukbir & Blanchard (1997) used the uncorrected (see Eke, Cole & Frenk 1996) HA91 temperature function, which gives an over-abundance of present-day clusters. This will feed through into the Ω_0 determination (equation 7 of Sadat et al.) and produce an over-estimate, although it is not clear by how much. The measurement of the L–T evolution found by Sadat et al. relies upon the correct choice of the slope for this relation. It is important because the more distant observed clusters are intrinsically hotter and more luminous than the nearby ones, and if the slope of the L–T relation (they choose $L \propto T^3$) is not accurate, then some spurious evolution (or lack of evolution) would be introduced because of the different types of clusters being probed at high and low redshifts. For the low-redshift clusters contained in their table 1 the mean temperature is 6.05 keV and the mean luminosity is 15.9×10^{37} W. From table 2 in their paper, the mean temperature and luminosity for clusters satisfying $0.4 < z < 0.6$ are 7.13 keV and 55×10^{37} W. If the L–T relation is non-evolving, then this suggests that $L \propto T^{\sim 7}$. (This exponent is still > 6 if the one high-redshift cooling flow cluster RX J1347.5 − 1145 is removed from this calculation.) So there is an apparent inconsistency in the method that is likely to have an impact on the derived value of Ω_0. Their fig. 3 and equation (5) suggest that if the high-z clusters are biased to have large luminosities, then this would cause Ω_0 to be over-estimated.

6 ORDER STATISTICS AND THE *EMSS* CLUSTER SAMPLE

A number of recent papers have reported the existence of large mass concentrations at redshifts above 0.5 (Luppino & Gioia 1995; Donahue 1996; Luppino & Kaiser 1997; Donahue et al. 1998). Very often these findings are accompanied by a claim that the existence of such objects proves troublesome for hierarchically clustering models of structure formation, particularly if $\Omega_0 = 1$. However, the magnitude of this difficulty is not quantified. The purpose of this section is to propose and then apply a method by which the extent of the problem can be gauged. To this end, the question: 'What is the expected redshift of the nth furthest galaxy cluster with a temperature above kT?' will be addressed. The answer will depend sensitively upon Ω_0 because of the dependence of the growth rate on Ω_0. Thus one should be able to use the observations of hot, distant clusters to discriminate between different values of Ω_0. More specifically, given that any observational survey is likely to be less than 100 per cent complete, the presence of a hot, massive cluster can be used to set an upper limit on Ω_0.

6.1 Method and application

The Press–Schechter expression for the abundance of haloes as a function of mass has been tested using large N-body simulations out to about $z = 0.5$ for haloes with masses corresponding to $kT \sim 5$ keV in an $\Omega_0 = 1$ universe (e.g. Eke et al. 1996). It appears to provide a good description of the cluster mass function over this range of redshifts when the spherical collapse threshold density is used. The more recent, and larger, simulation of Tozzi & Governato (1998) suggests that the Press–Schechter equation over-estimates the observed evolution in very massive haloes. However, it is not yet clear how much of this apparent discrepancy results from their particular choice of groupfinder. Whilst the theoretical expectation is still somewhat uncertain for very rare objects at $z \gtrsim 0.5$, this is an issue that can be addressed in the near future with very large volume dark matter simulations (e.g. Evrard et al., in preparation), so this need not be an insurmountable barrier to the usefulness of the approach described here.

As described in Section 2, the halo mass function is obtained by using the simple spherical collapse model in conjunction with the Press–Schechter expression. Additionally, $\bar{\beta}_{\mathrm{TM}} = 1$ will be assumed to hold at all redshifts, along with a 20 per cent scatter about this mean value. Using the results of Eke et al. (1996), the normalization of the mass fluctuation spectrum will be taken as 0.50 ± 0.04 for the $\Omega_0 = 1$ model considered in this section. [Note that this is slightly different from the best-fitting value of 0.52 found by Eke et al. (1996). This new estimate takes into account both the systematic overestimation of σ_8 resulting from the measured temperature uncertainties (see table 1 of Eke et al. 1996) and another, slightly larger, term (neglected in their table) arising from scatter in the mass–temperature relation.]

From these stipulations it is possible to calculate the redshift distribution of all clusters hotter than a specified value. The probability that, from the population of clusters hotter than a particular temperature, a cluster is situated at a redshift no greater than z will be denoted by $P(\leq z) \equiv P(\leq z \,|\, kT > kT_{\mathrm{min}})$. This quantity is calculable from the model for any given temperature. For brevity and clarity, the temperature dependence is suppressed in the following expressions. Using this notation, the probability that the furthest cluster (at z_1) has a redshift greater than z can be written

$$P(z_1 > z) = 1 - P(z_1 \leq z) = 1 - [P(\leq z)]^N, \tag{6.1}$$

where N is the total number of clusters above the chosen temperature limit in the whole volume, given by the Press–Schechter formula. For a particular redshift distribution, larger N will probe further into the tail of the distribution, and z_1 will be expected to be larger. This procedure can be extended to give the redshift

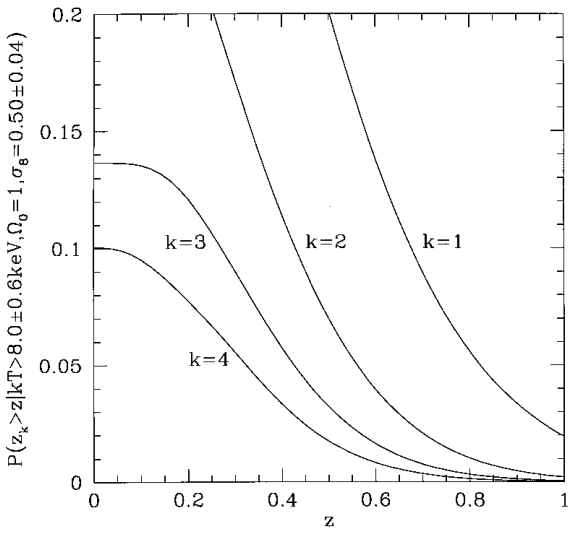

Figure 11. The probability that the kth furthest of all *EMSS* clusters with a temperature exceeding 8.0 ± 0.6 keV has a redshift larger than z, assuming a cosmological model with $\Omega_0 = 1$, $\sigma_8 = 0.50 \pm 0.04$ and $\Gamma = 0.25$. There is less than a 1 in 7 chance that three such objects will exist in an *EMSS* cluster survey area of sky, and only a probability of $\sim$0.02 that the third furthest hot cluster will have a redshift greater than 0.53.

distributions of the kth furthest cluster in the following manner. The probability that the kth furthest cluster (hotter than $kT_{\rm min}$) has a redshift greater than a particular value is given by

$$P(z_k > z) = 1 - P(z_k \leq z). \tag{6.2}$$

To calculate the last term in this equation, it is necessary to consider the various combinations of clusters that would give rise to $z_k \leq z$. This probability can then be written, using the combination function C,[2] as

$$P(z_k \leq z) = \sum_{j=0}^{k-1} {}^{N}C_j P(\leq z)^{N-j}[1 - P(\leq z)]^j, \tag{6.3}$$

and this, together with equation (6.2), gives $P(z_k > k)$. This probability will be very sensitive to both the model normalization σ_8 and the error in the measured cluster temperatures. Consequently, a marginalization technique allowing for Gaussian errors on both of these quantities has been employed. This involves integrating over all normalizations and temperatures, weighting with the probabilities that these are in fact the actual values of σ_8 and the lowest temperature of the clusters under consideration.

The three clusters that will be used in this analysis are MS 0015.9+1609 at $z = 0.54$, MS 0451.6–0305 at $z = 0.54$ and MS 1054.5–0321 at $z = 0.83$. *ASCA* temperatures of 8.0 ± 0.6 keV (Mushotzky & Scharf 1997), 10.4 ± 1.2 keV (Donahue 1996) and 14.7 ± 2.1 keV (Donahue et al. 1998) respectively have been found for these objects. Therefore, in the *EMSS* cluster sample, the third furthest cluster having a temperature greater than or equal to 8.0 ± 0.6 keV has redshift larger than 0.53. Given that these clusters were all found during a search containing only 735 deg^2 of sky, this value, rather than the entire 4π steradians will be used for calculating the model predictions.

6.2 Results

As can be seen in Fig. 11, the probability that three clusters with $kT \geq 8.0 \pm 0.6$ keV exist in an $\Omega_0 = 1$, $\sigma_8 = 0.50 \pm 0.04$, $\Gamma = 0.25$ model is less than 0.14. Furthermore, it is another factor of $\sim$6 less likely that the third most distant of these has a redshift of more than 0.53, as is observed. The conclusion from this exercise would appear to be that such a model can be ruled out at the 98 per cent confidence level. This would improve to $\sim$99 per cent if an extra *EMSS* cluster hotter than 8 keV were found at a redshift larger than 0.53. It is worth reiterating that this result would vary somewhat if the Press–Schechter treatment of the halo mass function is badly awry, or if the best-fitting σ_8 is underestimated because of a poor choice of the factor relating mass to temperature, $\beta_{\rm TM}$. It would therefore be premature to consider the existence of these hot clusters at high redshifts as being sufficient to rule out $\Omega_0 = 1$. Performing the same analysis for an $\Omega_0 = 0.52$, $\sigma_8 = 0.63 \pm 0.06$ model (keeping Γ fixed at 0.25) yields a probability of 0.38 for the third furthest of the *EMSS* $kT \geq 8.0 \pm 0.6$ keV clusters having $z > 0.53$.

7 OVERVIEW OF THE DIFFERENT TECHNIQUES

Having analysed cluster data in three distinct ways, it is worth discussing the strengths and weaknesses of the different methods that were employed in Sections 3, 4 and 6. While all of these techniques use similar input data to estimate Ω_0, they are sufficiently diverse to merit some discussion. Table 2 contains a summary of the main pros and cons of these approaches.

The main drawback of the first two methods, which is not as important in the order statistics approach, is the need for a statistically well-defined sample with well-understood selection effects. Given such catalogues, the particular data that are used by the χ^2 and maximum-likelihood (M.L.) techniques differ somewhat. In the former case, only the cluster temperatures and fluxes are important. The $1/V_{\rm max}$ estimator enables this method to sidestep the need for any cluster luminosity–temperature relation, apart from a minor incompleteness correction. However, the redundancy

Table 2. The main strengths and weaknesses of the three methods used here for constraining Ω_0 using cluster evolution.

Method	Strengths	Weaknesses
χ^2 (Section 3)	Utilises the cluster flux measurements.	Requires a statistical sample.
	Almost independent of L–T relation.	Results depend slightly on choice of z and T bins.
M.L. (Section 4)	All cluster redshifts are used.	Requires a statistical sample.
	No z or T bins are necessary.	Uncertainty introduced by L–T relation.
Order statistics (Section 6)	No need for a statistically well-defined data sample.	Model not yet tested with simulations.
	Independent of L–T relation.	Results are very sensitive to the assumed σ_8.

[2] The combination function is ${}^{N}C_j \equiv N!/[j!(N-j)!]$.

of the individual redshift measurements, other than in determining if a cluster should be included in the 'high-' or 'low-'z temperature function, leaves a certain freedom to choose what redshifts to assign to the fits. The choice of temperature bins can also alter the resulting Ω_0 determination to a small extent. In contrast, the M.L. method uses all the cluster temperatures and redshifts and avoids awkward binning problems. However, the limits of integration in equation (4.2), coming from the adopted ranges in z and T, do affect the most likely parameter values somewhat for the data used here. This comes about as a result of the peculiar redshift distribution of the high-z clusters, and the uncertainties in the selection function at the extreme temperatures and redshifts. Additionally, the price paid for not using the measured flux values is that one must adopt a luminosity–temperature relation (at all relevant redshifts), and any error in the assumed form of this relation will introduce a systematic error into the estimated Ω_0.

The difference between the derived best-fitting parameters from the χ^2 and M.L. techniques has non-negligible contributions from the systematic uncertainties just mentioned. Looking at the situation more positively, it is perhaps reassuring that, despite the various differences between the two methods, such similar results were returned.

An opportunity to win the jackpot is offered by the order statistics method; namely the chance to rule out $\Omega_0 = 1$ with observations of only a few very hot and distant clusters. However, the size of the payout for an apparently successful data set is not yet well defined because of the uncertainties in both the evolution of the cluster mass function and the mass–temperature conversion for such rare objects at such high redshifts. Nevertheless, these are both eminently measurable using numerical simulations. In particular, the 'Hubble volume' simulation performed by the Virgo consortium (Evrard et al., in preparation) should address the first of these issues in the near future. It is worth noting that incomplete virialization of large mass concentrations at high redshifts, or a boost in the emission-weighted temperature due to recent mergers should not, in principle, cause any difficulties for this method. This is because such effects are included in hydrodynamical simulations and would be calibrated through the assumed mean $\beta_{\rm TM}$ and the scatter around this value.

8 WHAT WENT WRONG?

Given that all 'right-minded' cosmologists *know* that $\Omega_0 = 1$, a pertinent question to ask at this point, on their behalf, is 'What has gone wrong?', i.e., what would it take for an $\Omega_0 = 1$ model to be favoured by cluster evolution. In this section consideration is given to the magnitude of the errors that are required in some of the preceding assumptions.

If Ω_0 is in fact unity, then it is very probable that at least one of the observations or the model used above is wrong. The first of these possibilities seems unlikely. An $\Omega_0 = 1$ model would require a systematic over-estimation of the high-redshift cluster temperatures by *ASCA* of about 25 per cent, or a corresponding underestimation of the low-redshift temperatures by this same amount. This corresponds to a systematic shift of all the cluster temperatures that is typically twice the quoted uncertainty and, as such, seems unlikely. Note, however, for 15 of the 25 HA91 clusters, the analysis of *ASCA* data by Markevitch et al. (1998) gave temperatures that were on average 6 per cent higher than the original determinations. While an increase of this size for the entire temperature function is not enough to be compatible with $\Omega_0 = 1$, it would nevertheless increase the most likely Ω_0 by $\sim$20 per cent.

Contamination of the X-ray emission by active galactic nuclei (AGN) or cooling flows would alter the mass–temperature conversion. The effect of AGN contamination is to increase the emission-weighted temperature. Cooling flows have the opposite effect. These potential complications are better addressed from the point of view of decontaminating the data, rather than adding extra processes into the numerical simulations, so will be considered as 'observational' problems. The likelihood of any interloping AGN in the high-redshift sample is very low, and high-resolution images show no evidence for such contamination. More important is the effect of cooling flows on the two different redshift samples. If cooling flows were more prevalent in the low-redshift sample than the high-redshift one, then allowing for them would result in an increased separation of the two temperature functions, thus favouring higher Ω_0. By fitting single-temperature isothermal models to *ASCA* data before and after excising the 'cooling flow' regions, Markevitch et al. (1998) showed that, for the 15 low-z clusters in common with HA91, the decontaminated emission-weighted temperature is, on average, 6 per cent larger than the contaminated temperature. For the most discrepant single cluster, the effect was 5 times as great. Allen (1998) has performed a similar analysis including two of the Henry (1997) high-z clusters, and finds an increase in the temperature by 15 and 24 per cent when a cool component is removed. There are two simple reasons why one might expect cooling flows to be more prominent in the *EMSS* high-z sample than in the HA91 catalogue. First, at high redshift, gas densities are larger and cooling times are shorter. Secondly, the *EMSS* selection algorithm tends to favour clusters that have centrally peaked emission, with only those exceeding a flux threshold in a 2.4×2.4 arcmin^2 detect cell being included in the catalogue. If the results of Allen (1998) are typical of the whole Henry (1997) sample, then the effect of cooling flow decontamination would be to increase the high-redshift cluster temperatures by more than the low-redshift ones. This would overcompensate for the systematic temperature shift in the low-redshift sample, leading to an overall estimate of Ω_0 that is about 20 per cent *lower* than the value found in Section 4, where these considerations were neglected.

As was discussed in Section 4, a 10 per cent incompleteness in the low-redshift sample only increases Ω_0 by 0.06, so this is not a sufficiently large effect to help the critical density model. Independent checks are available on the sample completenesses. These come from the comparison of luminosity functions obtained from the cluster catalogues used here with those from the larger *ROSAT* cluster samples at low (Ebeling et al. 1997) and high (Rosati et al. 1998) redshifts. *ROSAT* does not detect enough very luminous clusters to compare with the majority of the luminosity range of the *EMSS* high-z sample, because of the smaller fraction of sky it surveyed. Nevertheless, where an overlap in luminosity exists, there is agreement between the cluster abundances in the different surveys. These comparisons have enough statistical uncertainty to make them reassuring rather than conclusive. There could still plausibly be a $\sim$40 per cent difference between the various samples. In order to favour $\Omega_0 = 1$ though, there would need to be a significantly greater incompleteness in the low-redshift sample than in the more distant one, and this seems unlikely.

The considerations in the preceding few paragraphs suggest that, if anything, relative to the results found in Sections 3 and 4, lower rather than higher values of Ω_0 would be favoured by potential 'observational' systematic effects. Thus, if the data used in this paper are the product of an $\Omega_0 = 1$ universe, then it seems that the finger of suspicion should point firmly in the direction of the modelling of cluster evolution.

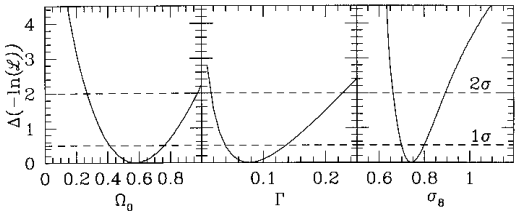

Figure 12. Δ (−ln likelihood) for Ω_0 (left panel), Γ (middle) and σ_8 (right), marginalized over the other two parameters in each case. Dashed lines at 1 and 2σ significance are shown, and the top of each panel corresponds to 3σ for one interesting parameter. The curves are calculated assuming that the collapse threshold is given by $\delta_{\rm eff} = 1.48(1+z)^{-0.06}$ rather than the spherical collapse $\delta_{\rm c}$.

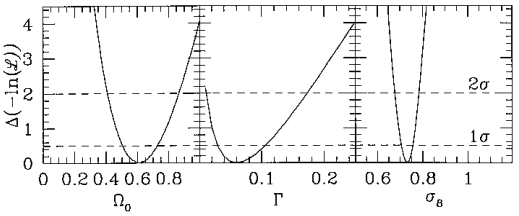

Figure 13. As for Fig. 12, but with the redshift information for the nine $z > 0.4$ *EMSS* clusters included in the likelihood calculation.

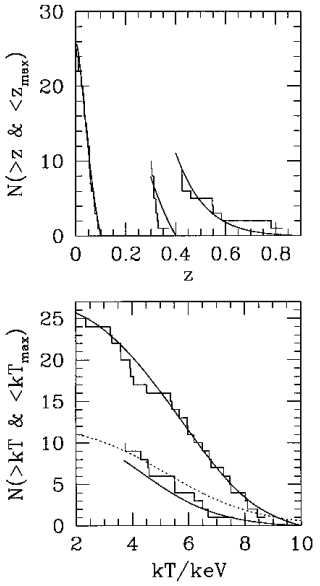

Figure 14. Marginalized distributions of clusters calculated assuming that the threshold varies with redshift according to $\delta_{\rm eff}$, and using the nine $z > 0.4$ extra *EMSS* clusters. Smooth curves are shown for the most likely model, namely $\Omega_0 = 0.62$, $\Gamma = 0.06$ and $\sigma_8 = 0.53$. The dotted curve in the temperature panel corresponds to the model prediction for the distribution of the temperatures that are yet to be measured. The stepped curves represent the observed cluster distributions.

While the statement that the Press–Schechter expression provides a good description of the mass function of galaxy clusters has stood up to much scrutiny, the recent report by Tozzi & Governato (1998) suggests that it over-estimates the actual evolution for $\Omega_0 = 1$. Their simulation is of a cube of side $500\,h^{-1}$ Mpc, and thus allows the evolution of very rare objects to be traced back to higher redshifts than was possible with the smaller volumes used in previous numerical studies. These authors suggest that the spherical collapse threshold $\delta_{\rm c}$ should be replaced by $\delta_{\rm eff} = 1.48(1+z)^{-0.06}$. This result appears to be slightly discrepant with previous findings where comparison is possible, and may just be an artefact of the groupfinder that was employed (see Cole & Lacey 1996 for more details). Nevertheless, it is worthwhile investigating the possibility that an evolving threshold may be required. Assuming that the expression for $\delta_{\rm eff}$ is applicable to all $\Lambda_0 = 0$ models (similar redshift evolution is found in a large $\Omega_0 = 0.3$ CDM simulation; Governato, private communication), the effect of such a varying threshold on the most likely value of Ω_0 can be investigated using the likelihood procedure described in Section 4. The resulting marginalized likelihoods are shown in Fig. 12. Whilst the most likely value of Ω_0 has only increased to 0.58, the $\Delta(-\ln\mathcal{L})$ required to reach $\Omega_0 = 1$ is now just 2.2, i.e., only $\sim 2\sigma$. Although this gives the impression that a small hit has been scored on the good ship $\Omega_0 < 1$, the captain might retaliate by pointing out that the *EMSS* survey found clusters with $z > 0.4$ and, given that the Tozzi & Governato $\delta_{\rm eff}$ fitted their simulated mass function out to a redshift of one, these distant objects can now be included in the likelihood calculation. Temperatures have yet to be measured for all of these clusters, but they do have known redshifts, so an additional contribution to the likelihood is computed by replacing the a in equation (4.2) by the integral of a over all cluster temperatures (2–20 keV in practice) and just comparing the probability of finding clusters at the observed redshifts. Additionally, the value of $f_{\rm clus}/f_{\rm det}$ is taken to be 1.75, independent of redshift for the $z > 0.4$ *EMSS* clusters. The nine identified *EMSS* clusters[3] with $z > 0.4$ and their corresponding redshifts are taken from Gioia & Luppino (1994, 1995), and the marginalized likelihoods resulting from their inclusion are shown in Fig. 13. It should be noted that there are also nine unidentified *EMSS* sources (Gioia & Luppino 1994), some of which might contribute to this list, and consequently reduce the estimated value of Ω_0 from that found here. The most likely parameters change only slightly, becoming $\Omega_0 = 0.62$, $\Gamma = 0.06$ and $\sigma_8 = 0.53$. Furthermore, the inclusion of the more distant clusters significantly decreases the statistical uncertainties on the most likely parameters, such that $\Omega_0 = 1$ is now excluded at a higher confidence level than was the case with the original default assumptions, despite the favourably evolving $\delta_{\rm eff}$. Distributions of the numbers of clusters marginalized with respect to either redshift or temperature are shown in Fig. 14. As the temperatures have yet to be measured for all of the highest redshift clusters, this model 'prediction' is shown as a dotted line.

In addition to any uncertainties in the accuracy of the Press–Schechter description of the mass function, there is some leeway in the conversion from mass to temperature that may effect the most likely Ω_0. There are at least five options for tinkering in an attempt to salvage $\Omega_0 = 1$.

(1) Evolution of the scatter in the cluster mass–temperature conversion or in the size of the observational errors in the measured temperatures would give rise to a systematic error in the estimation of Ω_0. It has been assumed that the intrinsic scatter is unchanging, and that the low- and high-redshift temperature errors are similar (which the quoted values suggest they are). If these scatters at high redshift implied that a Gaussian smoothing width of $0.4T$ rather than $0.2T$ was appropriate, then even the $\Omega_0 = 1$ model cluster temperature function would appear not to evolve. However, for the

[3] Recent HRI data show that MS 1610.4+6616 is a point source (Henry, in preparation) and it is not included.

mass–temperature relation, the low-Ω_0 simulations of Eke et al. (1998) show no significant evolution in the scatter over this range of redshifts (see Fig. 1). The observational uncertainties are relatively small and only slightly larger for the high-z sample. The conclusion is therefore that such an escape for $\Omega_0 = 1$ is not easily arranged.

(2) Evolution of μ, the mean molecular weight of the intracluster gas, has been ignored in the modelling. If it were 25 per cent larger at $z = 0.33$ than at $z = 0$, then the model predictions for $\Omega_0 = 1$ would show no evolution over this redshift range. This change in μ is both extreme and in a counter-intuitive direction. Mushotzky & Loewenstein (1997) recently used *ASCA* data to show that the iron abundance in the intracluster medium (ICM) does not evolve over the range $0 < z \leq 0.3$. Also, Kauffmann & Charlot (1998) applying a semi-analytical approach to the formation and evolution of elliptical galaxies, concluded that the metallicity of the ICM is approximately constant out to $z > 1$. This avenue for saving $\Omega_0 = 1$ also seems closed.

(3) Evolution of $\beta_{\rm TM}$ to the extent described for μ in (2) above would also make $\Omega_0 = 1$ compatible with the observations. For this, $\beta_{\rm TM}$ would need to be 25 per cent *smaller* at the larger redshift. As shown by the simulations of Eke et al. (1998) (see Fig. 1) this amount of evolution is difficult to justify and, if anything, $\beta_{\rm TM}$ at $z = 0.33$ is a few per cent larger than at low redshift. For the various cosmologies studied numerically by Bryan & Norman (1998), a similar lack of evolution was also found (see their fig. 4). This suggests that such a route will not assist $\Omega_0 = 1$ models either, and that the most likely value for Ω_0 quoted here may, if anything, be slightly biased high.

(4) One clear deficiency of the hydrodynamical simulations that have been used to relate virial mass to emission-weighted X-ray temperature is the lack of any heating of the intracluster gas by supernovae. That this is a problem becomes apparent when the simulated cluster luminosity–temperature relation is compared to the observed one. Whilst the models and scaling laws give $L \propto T^2$, the observations suggest a steeper dependence of luminosity on temperature (see equation 3.3). Allen & Fabian (1998) find that subtracting the cooling flow contribution to the X-ray emission can leave $L \propto T^{\sim 2}$. However, a similar study by Markevitch (1998) concluded that, in order to produce this shallow slope, some feedback is still necessary even after the cooling flow correction has been applied. NFW showed that by pre-heating gas in the manner suggested by Evrard & Henry (1991), low-temperature clusters in their simulations could be warmed up enough, along with a corresponding decrease in luminosity as a result of less dense cores, to produce a sufficiently steep luminosity–temperature relation to match observations. To obtain a very crude idea of the maximum extent to which such a change will affect the evolution of the $\Omega_0 = 1$ temperature functions, a simple mapping of temperature has been applied to the no-pre-heating value, $(kT)_0$, to give a 'feedback' temperature, $(kT)_1$. The mapping that has been adopted is

$$\log_{10}(kT)_1 = 0.57\ \log_{10}(kT)_0 + 0.34. \qquad (8.1)$$

This route for converting the simulated clusters to lie on the observed luminosity–temperature relation is extreme in its effect on the cluster temperatures. In practice, one would expect any energy injection to heat the gas *and* decrease the central density. As a result, the simulated clusters would fall on to the observed $L_{\rm x}$–$T_{\rm x}$ relation more as a result of decreasing luminosity than increasing temperature, as is assumed for the mapping above. Fig. 15 shows the predictions before and after 'feedback' when the same distortion is applied to both high- and low-redshift models.

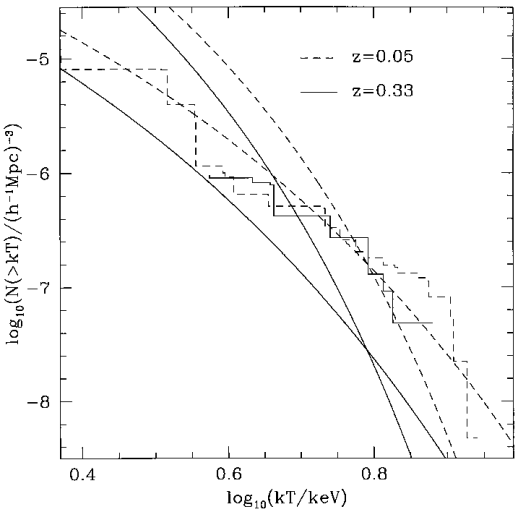

Figure 15. The temperature functions for an $\Omega_0 = 1$, $\sigma_8 = 0.52$ and $\Gamma = 0.25$ model are shown with solid and dashed lines for $z = 0.33$ and 0.05 respectively. In each case, the curves resulting from applying the temperature mapping of equation (8.1) are also shown. These are steeper than the original predictions. Stepped curves show the observationally determined temperature functions.

With the 'feedback' essentially just heating the cooler clusters, it produces steeper cumulative temperature functions, thus favouring lower Γ values. (It is worth noting that if the lower temperature clusters were preferentially contaminated by cooling flows, then the estimated Γ would be biased low, but Markevitch 1998 reports that slightly the reverse is seen in his sample of nearby clusters.) Interestingly, the extreme feedback simulations of Metzler & Evrard (1994) increased the gas temperature of a 5.6-keV cluster by ~15 per cent. This fractional change is reached with the above mapping only for clusters cooler than ~4.5 keV. Despite all of this, the predicted amount of evolution still exceeds that observed. Only if such a prescription were proscribed for the high-redshift sample alone would feedback be effective in reducing the amount of evolution seen in $\Omega_0 = 1$ models.

(5) The effects of a two-phase intracluster gas medium or magnetic fields are also missing from the hydrodynamical simulations used to normalize the mass–temperature relation. While it seems unlikely that these should have a different effect on the two redshift ranges considered here, they could still bias the best-fitting parameters, as was illustrated in Section 4, by shifting a different part of the mass function into the observed range of temperatures. The amount by which $\beta_{\rm TM}$ can be affected is roughly constrained by comparisons between weak lensing masses and X-ray masses. Current results (Smail et al. 1997; Allen 1998) appear to imply that this additional physics is not sufficiently misleading to allow $\Omega_0 = 1$ to be consistent with the lack of evolution of the cluster number density.

9 CONCLUSIONS

In this paper the value of the density parameter Ω_0 has been constrained using three different, yet similar, methods. The results are entirely consistent with those presented by Henry (1997). Combining the results from Sections 3 and 4 gives the most likely parameters as $\Omega_0 \approx 0.43 \pm 0.25$, $\Gamma \approx 0.08 \pm 0.07$ and $\sigma_8 \approx 0.67 \pm 0.1$ if $\Lambda_0 = 0$. The inclusion of a non-zero cosmological constant has very little effect, leading to $\Omega_0 \approx 0.36 \pm 0.25$, $\Gamma \approx 0.09 \pm 0.08$

and $\sigma_8 \approx 0.75 \pm 0.15$. Apart from the difficulty arising because of the peculiar redshift distribution of the Henry (1997) sample, none of the systematic effects that have been considered alter the best-fitting Ω_0 by more than one of the statistical standard deviations quoted above. Unless an important systematic error or uncertainty has been overlooked in this analysis, these results would appear to be limited by a lack of data, so, while this preliminary study suggests that $\Omega_0 = 1$ is still bobbing about in the water at a rejection level of $2–3\sigma$, a larger sample of clusters would offer the opportunity, with this method alone, to sink it properly. Enough ammunition should be provided by the upcoming X-ray telescope missions *XMM* and *AXAF*.

ACKOWLEDGMENTS

Doug Burke and Peter Coles are thanked for helpful discussions. George Efstathiou is thanked for providing a speedy computer. VRE, SC and CSF acknowledge the support of PPARC post-doctoral, advanced and senior fellowships. JPH was supported by NASA grants NAG 5-2523 and NAG 5-4828.

REFERENCES

Allen S. W., 1998, MNRAS, 296, 392
Allen S. W., Fabian A. C., 1998, MNRAS, submitted (astro-ph/9802218)
Bahcall N. A., Fan X., Cen R., 1997, ApJ, 485, L53
Bardeen J. M., Bond J. R., Kaiser N., Szalay A. S., 1986, ApJ, 304, 15
Blanchard A., Bartlett J. G., 1998, A&A, 332, L49
Borgani S., Gardini A., Girardi M., Gottlöber S., 1997, New Astron., 2, 119
Bower R. G., 1997, MNRAS, 288, 355
Bryan G. L., Norman M. L., 1998, ApJ, 495, 80
Bryan G. L., Cen R., Norman M. L., Ostriker J. P., Stone J. M., 1994, ApJ, 428, 405
Burke D. J., Collins C. A., Sharples R. M., Romer A. K., Holden B. P., Nichol R. C., 1997, ApJ, 488, L83
Carlberg R. G., Yee H. K. C., Ellingson E., Abraham R., Gravel P., Morris S. L., Pritchet C. J., 1996, ApJ, 462, 32
Carlberg R. G., Yee H. K. C., Ellingson E., 1997a, ApJ, 478, 462
Carlberg R. G., Morris S. L., Yee H. K. C., Ellingson E., 1997b, ApJ, 479, L19
Cen R. Y., Ostriker J. P., 1994, ApJ, 429, 4
Colafrancesco S., Mazzotta P., Vittorio N., 1997, ApJ, 488, 566
Cole S., Lacey C., 1996, MNRAS, 281, 716
David L. P., Slyz A., Jones C., Forman W., Vrtilek S. D., 1993, ApJ, 412, 479
Donahue M., 1996, ApJ, 468, 79
Donahue M., Voit G. M., Gioia I., Luppino G., Hughes J. P., Stocke J. T., 1998, ApJ, in press
Ebeling H., Edge A. C., Fabian A. C., Allen S. W., Crawford C. S., Böhringer H., 1997, ApJ, 479, L101
Edge A. C., Stewart G. C., Fabian A. C., Arnaud K. A., 1990, MNRAS, 245, 559
Efstathiou G., Bond J. R., White S. D. M., 1992, MNRAS, 258, L1
Efstathiou G., Frenk C. S., White S. D. M., Davis M., 1988, MNRAS, 235, 715
Eke V. R., Cole S., Frenk C. S., 1996, MNRAS, 282, 263
Eke V. R., Navarro J. F., Frenk C. S., 1998, ApJ, in press (astro-ph/9708070)
Evrard A. E., 1989, ApJ, 341, L71
Evrard A. E., 1990, ApJ, 363, 349
Evrard A. E., Henry J. P., 1991, ApJ, 383, 95
Evrard A. E., Metzler C. A., Navarro J. F., 1996, ApJ, 469, 494
Frenk C. S., White S. D. M., Efstathiou G., Davis M., 1990, ApJ, 351, 10
Frenk C. S., Evrard A. E., White S. D. M., Summers F. J., 1996, ApJ, 472, 460
Frenk C. S. et al., 1998, ApJ, submitted
Gioia I. M., Luppino G. A., 1994, ApJS, 94, 583
Henry J. P., 1997, ApJ, 489, L1
Henry J. P., Arnaud K. A., 1991, ApJ, 372, 410 (HA91)
Henry J. P., Gioia I. M., Maccacaro T., Morris S. L., Stocke J. T., Wolter A., 1992, ApJ, 386, 408
Hjorth J., Oukbir J., van Kampen E., 1998, MNRAS, in press (astro-ph/9802293)
Kaiser N., 1986, MNRAS, 222, 323
Kaiser N., 1991, ApJ, 383, 104
Kauffmann G., Charlot S., 1998, MNRAS, 294, 705
Kitayama T., Suto Y., 1997, ApJ, 490, 557
Lacey C., Cole S., 1994, MNRAS, 271, 676
Lilje P. B., 1992, ApJ, 386, L33
Luppino G. A., Gioia I. M., 1995, ApJ, 445, L77
Luppino G. A., Kaiser N., 1997, ApJ, 475, 20
Markevitch M., 1998, ApJ, in press (astro-ph/9802059)
Markevitch M., Forman W. R., Sarazin C. L., Vikhlinin A., 1998, ApJ, in press (astro-ph/9711289)
Mathiesen B., Evrard A. E., 1998, MNRAS, 295, 769
Metzler C. A., Evrard A. E., 1994, ApJ, 437, 564
Monaco P., 1998, Fundam. Cosmic Phys., 19, 157
Mushotzky R. F., Loewenstein M., 1997, ApJ, 481, L63
Mushotzky R. F., Scharf C. A., 1997, ApJ, 482, L13
Navarro J. F., Frenk C. S., White S. D. M., 1995, MNRAS, 275, 720 (NFW)
Oukbir J., Blanchard A., 1992, A&A, 262, L21
Oukbir J., Blanchard A., 1997, A&A, 317, 10
Pen U., 1998, ApJ, 498, 60
Press W. H., Schechter P., 1974, ApJ, 187, 425
Reichart D. E. et al. 1998, ApJ, submitted (astro-ph/9802153)
Rosati P., Della Ceca R., Norman C., Giacconi R., 1998, ApJ, 492, L21
Sadat R., Blanchard A., Oukbir J., 1998, A&A, 329, 21
Smail I., Ellis R. S., Dressler A., Couch W. J., Oemler A., Sharples R. M., Butcher H., 1997, ApJ, 479, 70
Tozzi P., Governato F., 1998, in D'Odorico S. D., Fontana A., Giallongo E., eds, ASP Conf. Ser. Vol., The Young Unvisere. Astron. Soc. Pac., San Francisco, in press (astro-ph/9711258)
Tsuru T., Koyama K., Hughes J. P., Arimoto N., Kii T., Hattori M., 1996, in Watanabe T., Yamashita K., eds, The 11th International Colloquium on UV and X-ray Spectroscopy of Astrophysical and Laboratory Plasmas. Universal Academy Press, Tokyo, p. 375
van Haarlem M. P., Frenk C. S., White S. D. M., 1997, MNRAS, 287, 817
White III R. E., 1991, ApJ, 367, 69
White S. D. M., Efstathiou G., Frenk C. S., 1993, MNRAS, 262, 1023